2. Filippou V., Tsoumpas C. Recent advances on the development of phantoms using 3D printing for imaging with CT, MRI, PET, SPECT, and ultrasound // Medical Physics. – 2018. – Vol. 45, № 9.
3. Rooney M.K. Three-dimensional printing in radiation oncology: A systematic review of the literature // Journal of Applied Clinical Medical Physics. – 2020. – Vol. 21, № 8. – P. 15–26.
4. Dodziuk H. Applications of 3D printing in healthcare // Kardiochir Torakochirurgia Pol. – 2016. – Vol. 13, № 3. – P. 283–293.
5. Kozee M. Methodology for computed tomography characterization of commercially available 3D printing materials for use in radiology/radiation oncology // Journal of Applied Clinical Medical Physics. – 2023. – Vol. 24, № 6. – P. e13999.
6. Boström C., Messler O. Design and Evaluation of a 3D Printed Ionization Chamber, 2019.

Odii Christopher Joseph (Nigeria)
Tomsk Polytechnic University, Tomsk
Scientific supervisor: Korotkikh Alexander G., Sci.Dr, Professor

THERMAL ANALYSES OF UNIFORMLY HEATED FUEL PIN CELL, INVERTED CELL, AND DUAL SURFACE COOLED CELL GEOMETRIES USING COMSOL MULTI-PHYSICS

Abstract. This study examines the thermal performance of pin cells, inverted cells, and dual surface-cooled cells under high heat conditions. We analysed key thermal properties, including linear heat generation rate and heat flux, by applying a uniform volumetric heat generation rate (VHGR) of $4 \cdot 10^7$ W/m³ to a pin of length 0.1 m. The results revealed a radial temperature drop of 65 °C for the inverted fuel pin, 26 °C for the normal pin, and 11°C and 13°C for the inner and outer surfaces of the dual surface-cooled pin, respectively. Thus, the dual surface-cooled pin had the lowest thermal loss, while the inverted pin had the highest thermal loss, despite achieving a higher surface temperature than the maximum of the dual surface-cooled pin.

Introduction

The thermal behavior of fuel materials is critical for nuclear reactor core design due to the thermal stress experienced during operation. In land-based light water reactors, fuel is cladded within a rod, shielded by zirconium layers and a gas gap. In maritime nuclear reactors, cladding wear may occur from fretting between the spacer grid

and cladding due to ship vibrations [1]. To enhance the mechanical integrity of fuel rods, the concept of inverted core fuel was considered, which involves multiple coolant lines in the fuel block. This study employs the equivalent annulus approximation to accurately represent temperature fields within the fuel pin, applicable for a pitch-to-diameter ratio of around 1.4 [2]. Furthermore, dual surface cooled fuel pins present unique thermal hydraulic properties that require analysis to manage coolant flow effectively [3]. This work compares the thermal behavior of solid, internally cooled (inverted), and dual surface cooled fuel pins to evaluate their feasibility for reactor fueling while addressing limitations. Based on extensive UO_2 fuel experience, S. Kazimi et al. proposed an annular fuel concept with an additional cooling channel compared to traditional PWR fuel [4]. Annular fuel pellets with a core cavity have been used in several Russian VVER reactors to reduce temperature drops across the fuel.

Modeling Method

This calculation was done with COMSOL multiphysics as a validation of similar work with different modeling parameters done in 2017 [5]. The modeling tool used in COMSOL was the Conjugate heat transfer which include heat transfer in solid and fluid with a k-epsilon turbulent model attached. A time dependent solver was used to ascertain the time at which each of the simulating fuel models achieved maximum temperature. For this model, two (2) materials were created, namely the cladding and fuel materials, while water was selected from the in-built materials. An inflow, outflow and heat source were added to the heat transfer in solid and fluid, while an inlet and outlet options were added to the k-epsilon turbulent model. A 2D axisymmetric option was selected for the modeling geometry, and a 2D rectangle was created for the three (3) models. COMSOL automatically solves the 2D rectangular geometry into a 3D cylindrical figure with 2D and 3D options for temperature, pressure and velocity distributions.

Once the physics option was completed, the models were meshed using the normal meshing option with physics controlled mesh. Thereafter a time dependent solver was initiated.

Table 1

Modeling parameters of fuel rod and coolant

Parameter	Value	Parameter	Value
VHGR	$4 \cdot 10^7$ W/m^3	Coolant pressure outlet	$1.62 \cdot 10^7$ Pa
heat transfer coefficient	58000 W/m^{2}K	Clad density	6550 kg/m^3
Fuel pellet domain radius	0.0038 m	Clad specific heat, cp	285.8 J/kgK
Clad thickness	0.00075 m	Clad thermal conductivity	21.5 W/mK
Coolant thickness	0.001875 m	Fuel density	10950 kg/m^3
Rod length	0.1 m	Fuel specific heat capacity	236 J/kgK
Coolant inlet temperature	571 K	Fuel thermal conductivity	6 W/mK
Coolant inlet velocity	5 m/s		

Result and Discussion

The temperature distribution for the dual surface-cooled fuel peaked within 5 seconds of computation (Fig. 1).

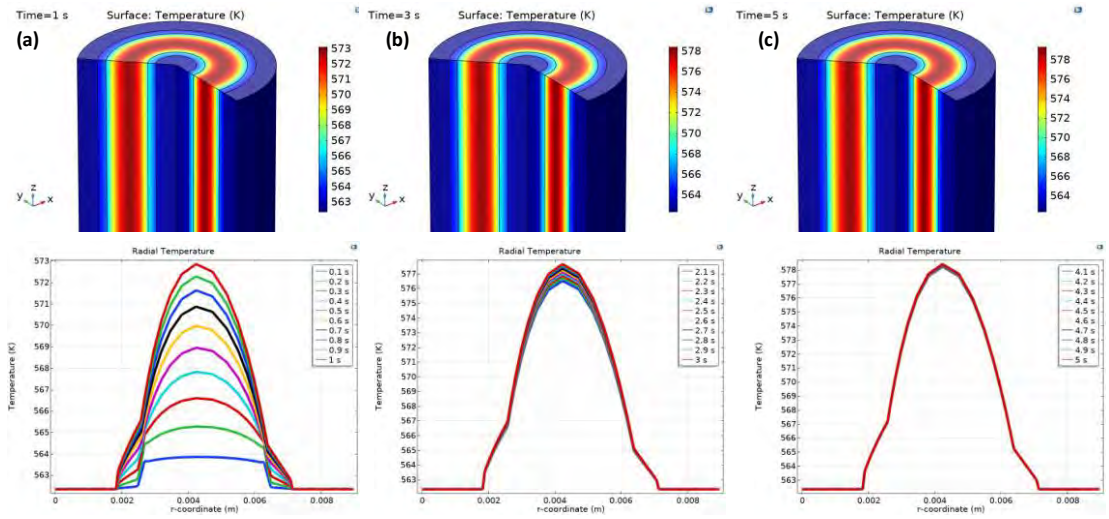

Fig. 1. Radial temperature distribution of dual surface cooled fuel at 1 sec, 3 secs and 5 secs

During the first second (Fig. 1(a)), the temperature changed rapidly, reflecting intense heat transfer. Between 2.1 and 3 secs (Fig. 1(b)), the temperature changes stabilized, indicating a gradual adjustment. By 4.1 to 5 seconds (Fig. 1(c)), temperatures converged at their maximum, confirming the iteration process's convergence. The solver took about 2 hours to complete the model, reaching a maximum temperature of 578.5 K, with inner and outer surface temperatures of 567.5 K and 565.5 K, respectively. Radial temperature drops within the fuel were 11 °C for the inner surface and 13 °C for the outer surface.

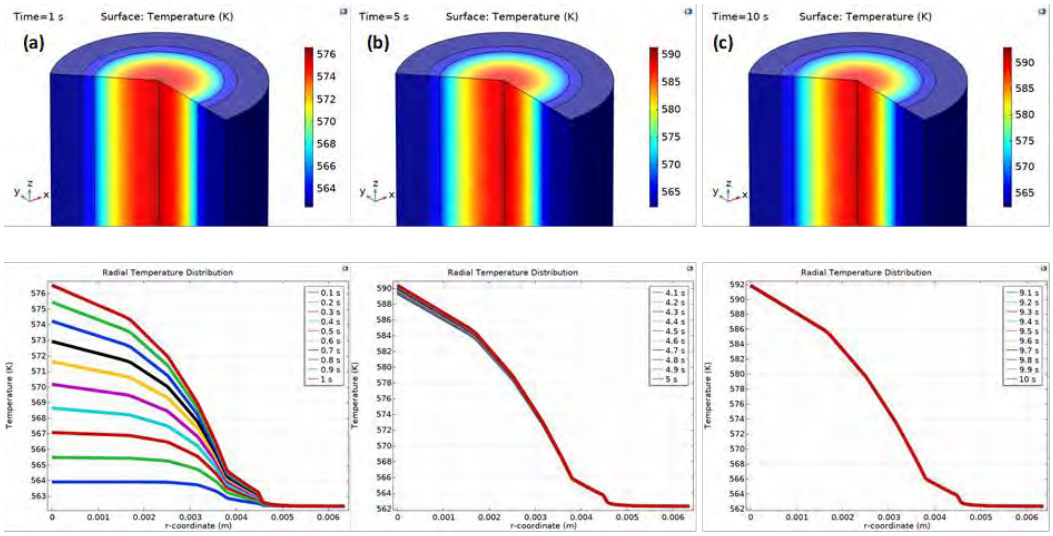

Fig. 2. Radial temperature distribution of outer cooled fuel at 1 sec, 5 secs and 10 secs

The temperature distribution of the outer cooled fuel reached a maximum within 10 secs, as illustrated in Fig. 2. Between 0.1 to 1 secs (Fig. 2 (a)), the heat transfer experienced rapid changes, showing noticeable temperature differences. From 4.1 to 5 secs (Fig. 2 (b)), the temperature changes became minimal, indicating a gradual approach to maximum temperature. By 9.1 to 10 secs (Fig. 2 (c)), temperatures consistently converged at the maximum of 592 K, with the outer surface at 566 K. The radial temperature drop within the fuel was 26 °C, significantly higher than that of the dual surface cooled fuel pin. This model took about 10 seconds to converge, twice as long as the dual surface cooled design, suggesting that larger cooled surface areas facilitate quicker heat transfer equilibrium.

For the temperature distribution of the inverted pin model (inner cooled fuel), it attained a maximum within 20secs of time dependent solving as seen in Fig. 3. From 0.1 sec to 1sec of iteration in Fig. 3 (a), the heat transfer within the fuel was rapidly changing with time, accounting for observable temperature difference between time-steps. From 4.1 secs to 5 secs in Fig. 3 (b), the temperature changes from one time-step to another was beginning to narrow, showing a gradual temperature difference between time-steps, it took a much longer time from 19.1 secs to 20 secs in Fig. 3 (c), for the temperatures of the entire time-steps to converge at the maximum. This behavior is due to the fact that the cooling area is much smaller when compared to the other two models, and hence, it took longer time for the heat transfer to attain equilibrium.

The maximum attainable temperature for this model was 655 K, while the inner surface temperature reached 590 K. There was a radial temperature drop of 65 °C within the fuel meat, which is significantly higher than that observed in the outer cooled and dual-surface cooled fuel pins. It took approximately 20 secs for the entire time step to converge at the maximum temperature, a duration that is also much longer than that for the outer cooled and dual-surface cooled configurations.

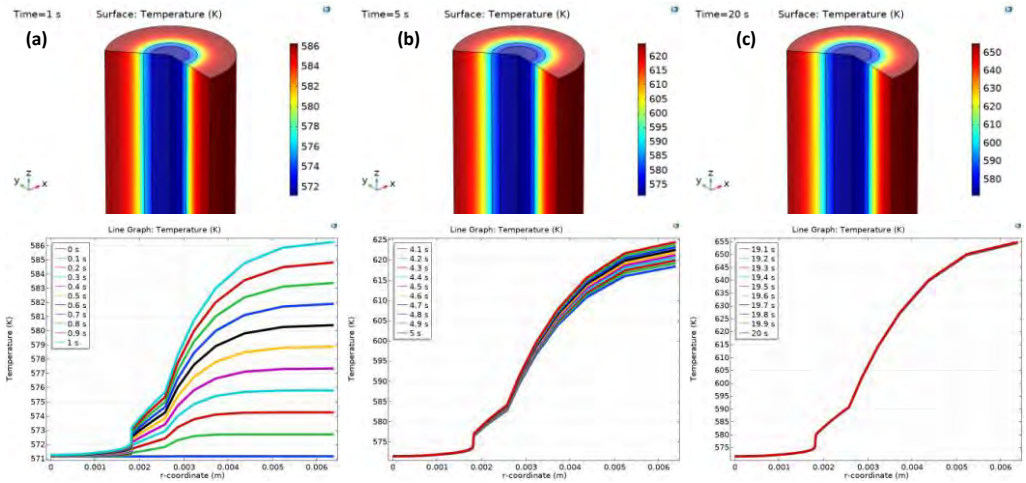

Fig. 3. Radial temperature distribution of inner cooled fuel at 1 sec, 5 secs and 20 secs

The coolant velocity for the outer-cooled fuel pin decreased near the cladding wall but increased midway between the cladding wall and the outermost part of the flow, as shown in Fig. 4(a). All coolant velocities reached a steady state at approximately 0.06 m before exiting the channel. For the dual surface cooled pin, the coolant velocity near both the inner and outer cladding walls decreased to around 0.05 m within the channel and then maintained a steady state until reaching the exit, as illustrated in Fig. 4(b).

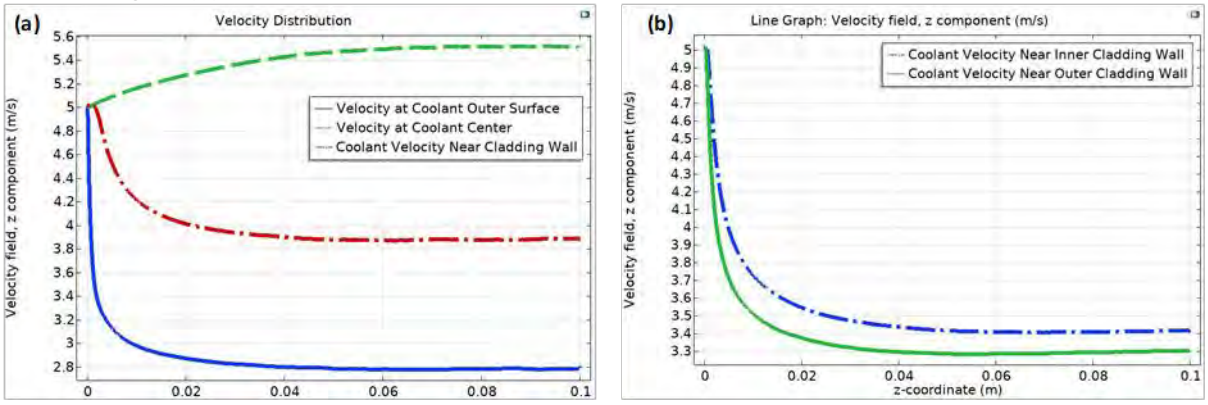

Fig. 4. Coolant velocity along z for (a) outer cooled model; (b) dual surface cooled model

Conclusion

In conclusion, when designing fuel pins, an inverted pin that is cooled solely from the inside will exhibit the highest centerline temperature (655 K) and highest temperature drop across the fuel (65 °C) compared to both a standard pin, which is (592 K) and (26 °C) and a dual-surface cooled pin which is (578.5 K) and temperature drop of 11 °C for the inner surface and 13 °C for the outer surface. This increased centerline temperature occurs because the inverted pin has a smaller cooled surface in comparison to the other two models. Conversely, the dual-surface cooled pin has the lowest centerline temperature, as its channel offers a significantly larger cooled surface.

The coolant velocity decreased near the inner and outer cladding walls, while maintaining a steady velocity halfway along the channel (0.05 m). This indicates that upon entering the channel, the velocity decreased due to turbulence, but after a short period, the flow stabilized as it moved toward the exit.

References

1. Ji Won Mun, Ho Jin Ryu, Finite Element Analysis of Unit Cell Inverted Core Fuel for Micro Lead-cooled Fast Reactor, Transactions of the Korean Nuclear Society Virtual spring Meeting May 13–14, 2021.
2. Todreas N.E., Kazimi M.S. Nuclear systems volume I: Thermal hydraulic fundamentals. – CRC press, 2015.

3. Wu Pan, et al. «Researches on special thermal hydraulic phenomena of annular fuel assembly by sub-channel analysis code-NACAF» Frontiers in Energy Research 9, 2021, P 696331.
4. Yuan Yi, M. S. Kazimi, and P. Hejzlar. «Thermomechanical performance of high-power-density annular fuel» Nuclear technology 160.1, 2007, P. 135-149.
5. Joseph Odii Christopher, Agyekum Ephraim Bonah, and Bright Kwame Afornu. «Effect of dual surface cooling on the temperature distribution of a nuclear fuel pellet» Key Engineering Materials 769, 2018 P. 296–310.

Rawand Samad Abdullah (Iraq)
Department of Chemistry, College of Science, Salahaddin University-Erbil, Kurdistan region, Erbil

ENTHALPY OF EVAPORATION FOR SOME AROMATIC COMPOUNDS AT STANDARD TEMPERATURE

Abstract: The three substituted quinolines, naphthalenes, and monosubstituted pyridines were collected phase transition enthalpies. The compounds' solvation enthalpy was estimated the additivity scheme. The evaporation enthalpy was estimated using gas chromatography, solution calorimetry, and the transpiration technique. The solution calorimetry-additivity scheme, the compounds' sublimation/vaporization enthalpy was calculated at 298.15 K.

Keywords: enthalpy of solution, enthalpy of solvation, solution calorimetry, enthalpy of evaporation.

Introduction

There are several uses for chemical organic aromatic molecules in both industry and medicine. Because pyridine derivatives have antibacterial, anti-poisoning, antidiabetic, and antiviral properties against HCV, they are used in a variety of medical applications, such as the production of medications against the influenza B-mass virus. Because of the diversity of their steric and electrical characteristics, they are also used in photochemistry, materials science, electro-optical display systems, solution research, and homogeneous catalysis [1]. In addition, the naphthalene derivatives have many applications in biotechnology and in industries like organic electronic applications [2]. Further, the quinolines were applied in preparation of drugs of Influenza B-Mass virus because they have antibacterial activity. Furthermore, the quinolines are used to treatment the diseases like cancer, malaria and anti-inflammatory, antidotes against poisoning, antidiabetic activities and antiviral HCV [3]. Therefore, thermochemical study on the chemicals like pyridines, naphthalines, and quinolines is essential before using them. The phase transition thermochemical